Superfast ion scattering by solar wind discontinuities

A. V. Artemyev,[1,2,*] A. I. Neishtadt,[2,3] A. A. Vasiliev,[2] V. Angelopoulos,[1] A. A. Vinogradov,[2] and L. M. Zelenyi[2,4]

[1]*Institute of Geophysics and Planetary Physics, University of California, Los Angeles, California, USA*

[2]*Space Research Institute RAS, Moscow, Russia*

[3]*Department of Mathematical Sciences, Loughborough University, Loughborough LE11 3TU, United Kingdom*

[4]*Moscow Institute of Physics and Technology (State University), 141700, Dolgoprudnyi, Moscow oblast, Russia*

(Received 31 May 2020; accepted 20 August 2020; published 2 September 2020)

Large-amplitude fluctuations of the solar wind magnetic field can scatter energetic ions. One of the main contributions to these fluctuations is provided by solar wind discontinuities, i.e., rapid rotations of the magnetic field. This study shows that the internal configuration of such discontinuities plays a crucial role in energetic ion scattering in pitch angles. Kinetic-scale discontinuities accomplish very fast ion pitch-angle scattering. The main mechanism of such pitch-angle scattering is the adiabatic invariant destruction due to separatrix crossings in the phase space. We demonstrate that efficiency of this scattering does not depend on the magnetic field component across the discontinuity surface, i.e., both rotational and almost tangential discontinuities scatter energetic ions with the same efficiency. We also examine how the strong scattering effect depends on the deviations of the discontinuity magnetic field from the force-free one.

DOI: 10.1103/PhysRevE.102.033201

I. INTRODUCTION

The supersonic solar wind is filled by large-scale magnetic field fluctuations, such as Alfven waves and solar wind discontinuities (SWD) [1,2]. Recent Parker Solar Probe observations found an abundance of such SWD at small radial distances from the Sun [3,4]. These fluctuations contribute significantly to the solar wind heating [5], as well as acceleration [6] and scattering of energetic ions [7,8]. Such scattering results in random jumps of ion pitch angles due to the ion interaction with magnetic field fluctuations [9], which are dominated by magnetic field rotations [10,11].

Energetic ion (more than a few keVs of thermal energy) scattering is responsible for the cross-field transport [12] affecting ion propagation time in the heliosphere [13] and ion spatial distributions [14]. The classical theory of ion scattering is based on consideration of an ensemble of random magnetic field fluctuations [7,8,15], whereas the internal structure of such fluctuations has not been studied in detail. Compressional fluctuations, e.g., high-β current sheets, are known to be effective ion scatters [16]. However, solar wind fluctuations are dominated by compressionless magnetic field rotations (so-called rotational SWD, see [1,10]), and there is no theory describing the role of the SWD internal structure in the ion scattering. This study focuses on the ion scattering by such SWD consistent with observed magnetic field configurations.

Figure 1 shows a typical example of rotational SWDs observed by the ARTEMIS spacecraft [17] at 1 AU. The magnetic field rotates while $|\mathbf{B}| \approx$ const [see Fig. 1(a)]: the reversal of the magnetic field component along the maximum variance direction, B_l is compensated by a peak of the absolute value of the intermediate variance direction component, B_m [see Fig. 1(b)]. Using the solar wind velocity projected onto the normal direction to the SWD surface, that of the minimum variance, $\mathbf{n}$ (e.g., Ref. [18]), we transform time to space r_n and normalize it to the proton inertial length $d_p = \sqrt{m_p c^2/4\pi n_p e^2}$, where n_p is the solar wind density. The spatial scale of this SWD is few d_p, and the current density peak reaches $j_m \approx (c/4\pi)\partial B_l/\partial r_n \sim 30$ nA/m^2 [Fig. 1(c)]. These are typical scale and j_m for the most intense SWDs with B_l magnitude B_0 comparable to the $|\mathbf{B}|$ [18–20]. Ion scattering is expected around the strongest magnetic field gradient [21,22], i.e., around the B_l reversal.

II. BASIC EQUATIONS

We fit the observed magnetic field around the discontinuity center (B_l reversal) by a simple model: $B_l \approx B_0(r_n/L)$, $B_n =$ const, $B_m = \sqrt{B_0^2 - B_l^2} \approx B_0(1 - r_n^2/2L^2)$, where L is the discontinuity thickness, $L \approx cB_0/4\pi j_m \approx 250$ km. The ion (of mass m and charge q) motion in such a field is given by the Hamiltonian:

$$H = \frac{1}{2m}p_n^2 + \frac{1}{2m}\left[p_l - \frac{qB_0}{c}\left(r_n - \frac{r_n^3}{6L^2}\right)\right]^2 + \frac{1}{2m}\left(p_m - \frac{qB_n}{c}r_l + \frac{qB_0}{c}\frac{r_n^2}{2L}\right)^2, \quad (1)$$

where momenta $\mathbf{p} = (p_l, p_m, p_n)$ are conjugate to coordinates $\mathbf{r} = (r_l, r_m, r_n)$. We introduce dimensionless variables $(x, z) = (r_l - p_m c/qB_n, r_n)/\sqrt{L\rho}$, $(p_x, p_z) = (p_l, p_n)/\sqrt{hm}$ (note $p_m =$ const because $\partial H/\partial r_m = 0$), $H \to H/h$, $\kappa = (B_n/B_0)\sqrt{L/\rho}$, where $\rho = \sqrt{2hmc}/qB_0$ and $h =$

*aartemyev@igpp.ucla.edu

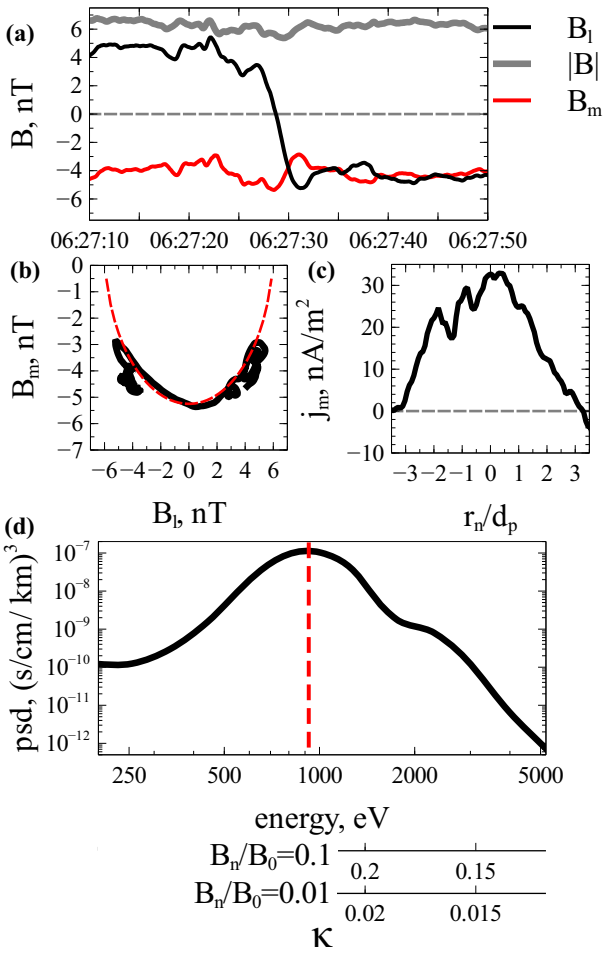

FIG. 1. Example of a discontinuity observed by ARTEMIS [17] on February 2, 2020: (a) magnetic field in the discontinuity coordinate system (**l** is the maximum variance direction, **m** is the intermediate variance direction), (b) magnetic field hodogram (B_l, B_m) and the circle $(B_m - 0.75\ \mathrm{nT})^2 + B_l^2 \approx 36\ \mathrm{nT}^2$ (red dased curve), (c) current density profile, (d) ion energy spectrum with the solar wind flow energy $m_p v_{sw}^2/2$ shown with red dashed line; two bottom axes show κ parameter calculated for the spectrum energy minus the flow energy, $\Delta E = E - m_p v_{sw}^2/2$ (ΔE is zero for ions moving with the solar wind; two B_n values are used for κ). We show κ for the energetic part of spectrum only as interaction of these ions with SWD is considered. Magnetic field at 0.25-s resolution is from the fluxgate magnetometer [23], whereas ions at 4-s resolution, the spin period, is from the electrostatic analyzer [24]. The local coordinate system and the current density are obtained from maximum variance analysis [25] and timing, respectively (see details in Ref. [18]). ARTEMIS data are processed with SPEDAS V3.1 [26]. Two ARTEMIS observations are not sufficient to accurately estimate the direction along the normal **n** to the SWD surface (see discussion in Ref. [27]), and thus we use a range of B_n values (normalized to the B_l magnitude) for the κ calculation in panel (d).

$(qB_0L/mc)^2 m$ (i.e., $\rho = L$ for this normalization) and rewrite Eq. (1) as:

$$H = \frac{1}{2}p_z^2 + \frac{1}{2}\left(p_x - z + \frac{z^3}{6}\right)^2 + \frac{1}{2}\left(\kappa x - \frac{z^2}{2}\right)^2. \quad (2)$$

The distinctive feature of Hamiltonian in Eq. (2) is the term $\sim z^3/6$ describing magnetic field B_m peak; previous analysis of ion motion was limited to Hamiltonians with $p_x^2/2$ [22,28] or $(p_x - z)^2/2$ [29,30] terms, describing discontinuities with $B_m = 0$ and $B_m = \mathrm{const}$. In this study we demonstrate that the new term $\sim z^3/6$ qualitatively changes the ion scattering efficiency.

In most discontinuities the observed $B_n/B_0 \ll 1$ [31], i.e., $\kappa \ll 1$ and variables $(\kappa x, p_x)$ change much slower than (z, p_z) [see the range of κ values in Fig. 1(d)]. This determines the character of the ion interaction with discontinuities. For frozen $(\kappa x, p_x)$, the Hamiltonian (2) describes periodic motion in the (z, p_z) plane with conserved generalized magnetic moment $I_z = (2\pi)^{-1} \oint p_z dz$. For slow changes of $(\kappa x, p_x)$ I_z remains conserved, now as an adiabatic invariant [32]. I_z only changes due to a significant change of the trajectory configuration [33]. The conservation of I_z and energy [Hamiltonian in Eq. (2) is conservative] is sufficient to fully integrate the ion motion, and thus without I_z destruction there is no ion scattering at discontinuities. Generally, the adiabatic invariant I_z is conserved with an exponential accuracy $\sim \exp(-\mathrm{const}/\kappa^2)$ [21,34,35], i.e., ion scattering is quite weak (slow). However, the Hamiltonian in Eq. (2) describes two different types of ion motions in the (z, p_z) plane [see Fig. 2(a) showing two types of phase portraits] and change of one type of motion to another type corresponds to an I_z jump of the order of $\sim\kappa$ or ~ 1 due to crossing of the separatrix demarcating phase domains with two types of motions [36–38].

Jumps of I_z due to separatrix crossings have been studied for special cases of the Hamiltonian of Eq. (2) with $\sim p_x^2/2$ [22] and $\sim(p_x - z)^2/2$ terms [30]. In both systems these jumps are found to be random with an amplitude $\sim\kappa$ and zero mean value, $\langle \Delta I_z \rangle = 0$, after averaging over many separatrix crossings, i.e., there is slow diffusion of I_z with variance $\langle (\Delta I_z)^2 \rangle \sim \kappa^2$ and diffusion rate $\langle (\Delta I_z)^2 \rangle/\tau \sim \kappa^3 \ll 1$ [39], where $\tau \sim 1/\kappa^2$ is the timescale between two separatrix crossings [timescale of the ion motion in the $(\kappa x, p_x)$ plane].

Besides the exponential $\sim \exp(-\mathrm{const}/\kappa^2)$ or slow $\sim\kappa^3$ destruction of I_z for systems with $\kappa \ll 1$, there also exists a so-called geometrical destruction (with $\langle \Delta I_z \rangle \sim 1$) predicted theoretically [40] and not yet found for conservative Hamiltonians describing ion interaction with discontinuities (see discussion in Ref. [30]). In this study we show that the term $\sim z^3/6$ (i.e., B_m peak) results in such geometrical I_z destruction and produces very fast ion scattering.

III. JUMPS OF THE ADIABATIC INVARIANT

To show the effect of I_z change due to separatrix crossings, we color the $(\kappa x, p_x)$ plane according to the phase portraits in a (z, p_z) plane. Note the two types of phase portraits correspond to two profiles of effective potential energy $U(z) = H - p_z^2/2$: There are two potential wells [one or two possible orbits in the (z, p_z) plane at fixed H] in the left portrait in Fig. 2(a), and there is a single potential well [one possible orbit in the (z, p_z) plane at fixed H] in the right portrait shown in Fig. 2(a). In Figs 2(c) and 2(d) the region with a single possible orbit is yellow and the region with two possible orbits is red (lines ℓ_{1-5} demarcate these regions). Orbits crossing ℓ_{1-4} do not change their potential well of $U(z)$, i.e.,

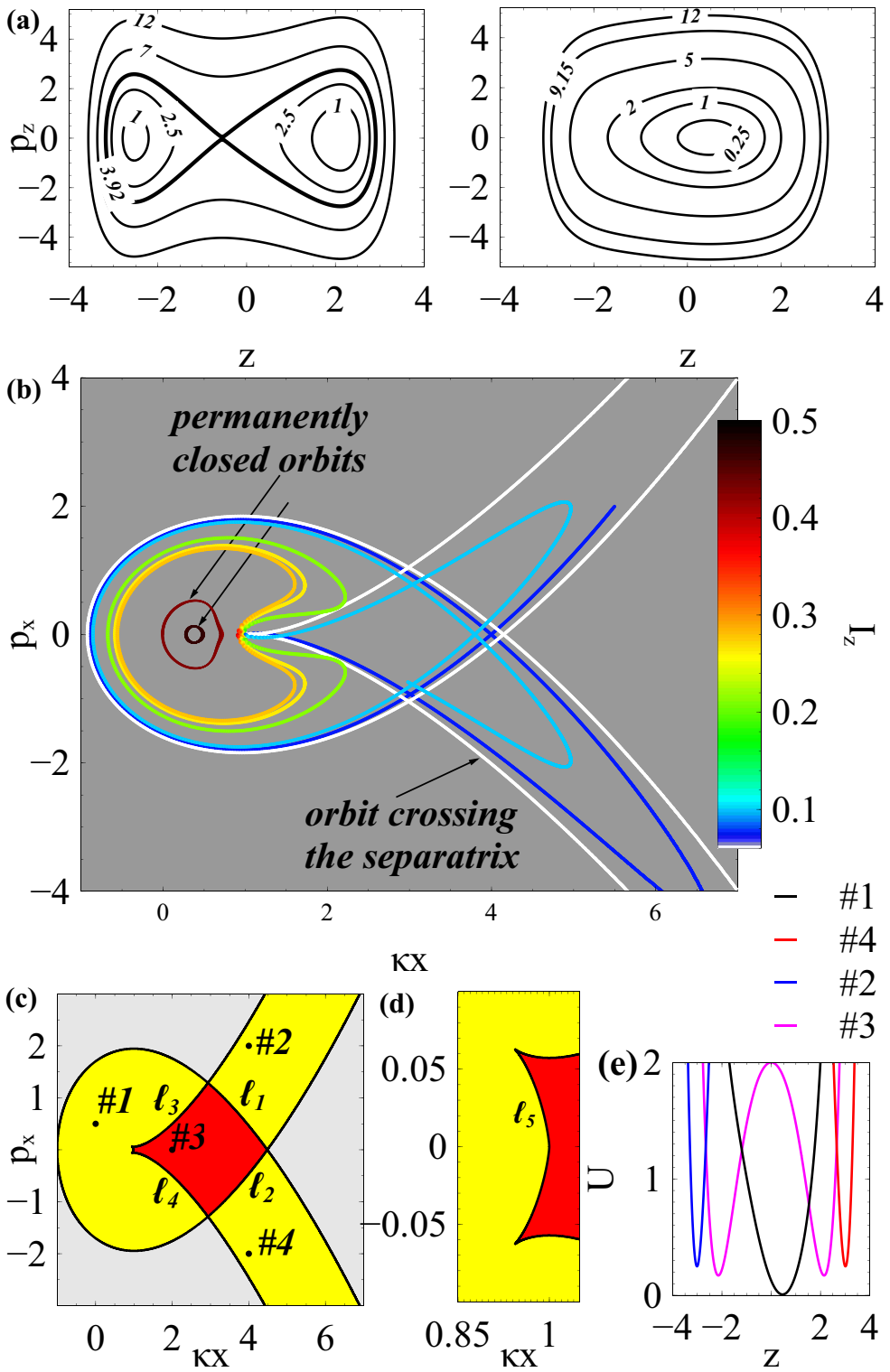

FIG. 2. Properties of Hamiltonian system of Eq. (2) for total energy $H = 1/2$. (a) Phase portraits of Hamiltonian (2) at frozen $(\kappa x, p_x)$: H values of each curve are shown in the plot; $\kappa x = 2.5$, $p_x = 1$ in the left panel and $\kappa x = 0$, $p_x = 0.5$ in the right panel. (b) Ion trajectories for many periods of slow motion in the $(\kappa x, p_x)$ plane ($\kappa = 0.01$); color shows instantaneous value of I_z; arrows show different types of orbits: Except for the permanently closed orbits that never cross the separatrix, all other curves are sections of the same orbit reflecting from ℓ_5 and changing I_z at these moments. All the orbits have $H = 1/2$ and initial $(\kappa x, p_x) = (5.5, 2.0)$, $(0.0, -3.5)$, $(0.0, 0.5)$. (c) Plane $(\kappa x, p_x)$ colored according to the type of motion in (z, p_z) plane with frozen $(\kappa x, p_x)$: Yellow denotes a single possible orbit in the (z, p_z) plane at fixed $H = 1/2$ (the right phase portrait in panel (a) or the left phase portrait in panel (a), but with only one orbit having $H = 1/2$), red denotes two possible orbits in the (z, p_z) plane at fixed $H = 1/2$ [the left phase portrait in panel (a)], and gray denotes the absence of solutions. (d) Zoomed-in section of (c) at $\kappa x \in [0.85, 1.05]$ and $p_x \in [-0.1, 0.1]$. (e) One-dimensional profiles of potential energy $U(z) = H - p_z^2/2$ at frozen $(\kappa x, p_x)$: Numbers correspond to # marks in (c).

the corresponding particles continue oscillating in the same well. Separatrix crossings occur when orbits cross (or reflect from) the boundary ℓ_5. Particles moving with κx decreasing at crossing ℓ_5 change oscillations in one of the two potential wells to oscillations covering the both wells (and vice versa for particles moving with κx increase). Particles moving with κx decrease and reflecting from ℓ_5 change oscillations in one of the two potential wells to oscillations in another well. Such crossings correspond to change of the well that results in I_z jump (this $2\pi\Delta I_z$ jump equals to the difference of areas of two regions surrounded by the separatrix in the (z, p_z) plane and does not depend on κ, see Ref. [33]). This is why I_z always changes when the orbit reflects from ℓ_5 in $(\kappa x, p_x)$ plane [and thus switches from oscillations in one well to oscillations in another well in (z, p_z) plane]: Figure 2(b) demonstrates the change of I_z (shown in color) for a single orbit.

There are two main populations of trajectories in the $(\kappa x, p_x)$ plane. The first consists of trajectories reflected from ℓ_5 curve and quickly scattered due to $\Delta I_z \sim 1$ jumps. The second consists of so-called closed trajectories trapped within the discontinuity, which never arrive close to ℓ_5 [see Fig. 2(b)]. Exchange between these two ion populations should be controlled by external forces and dissipative processes (e.g., wave-particle interactions [41] or discontinuity evolution [10,42]). Such evolution and (or) dissipation makes the system nonconservative (i.e., particle energy changes during particle interaction with the discontinuity) and results in evolution of the boundary separating these two populations in the phase space [39,43]. A third (minor) population of quasiclosed trajectories that cross ℓ_5 rarely is quite small for Hamiltonian (2). Let us discuss peculiarities of these three populations regarding their interaction with ℓ_5.

The first two populations are as follows: (i) regular trajectories never approaching ℓ_5 with $I_z \approx$ const [in the $(\kappa x, p_x)$ plane these trajectories occupy region located to the left from ℓ_5] and (ii) transient trajectories reflecting from ℓ_5. Due to geometrical I_z jumps trajectories of this latter population are characterized by rapid destruction of I_z invariant. The population (iii) consists of ion trajectories that cross ℓ_5. We can call these trajectories quasiregular, because ions on these trajectories can spend a long time on the boundary of the regular trajectory region ($I_z \approx$ const for this motion), but rarely does such a trajectory cross ℓ_5 and go to the $(\kappa x, p_x)$ region of transient trajectories. Figure 3 shows an example of this quasiregular behavior: The ion moves along a quasiclosed orbit on the left from ℓ_5 (within the region of closed trajectories) for quite a long period of time; then, finally, the weak scattering in I_z results in crossing ℓ_5 and escape into the region of transient trajectories. An analog of this orbit with the ion moving in the opposite direction would be represented by the ion approaching ℓ_5 from the right and then crossing ℓ_5. Note that the absolute majority of trajectories approaching ℓ_5 from the right are transient trajectories, which are reflected from ℓ_5.

To estimate the amount of such quasiregular trajectories we use the Poincaré section technique: We run 10^5 trajectories with initial 10 values of $\kappa x \in [-1, 1]$, $p_x = 0$, and uniformly distributed z; then we plot the points where the trajectories cross the $z = 0$ plane with $p_z > 0$. These points are spread within the circle $(\kappa x)^2 + p_x^2 = 2H$ and their distribution shows the three populations of trajectories (see Fig. 4): (i)

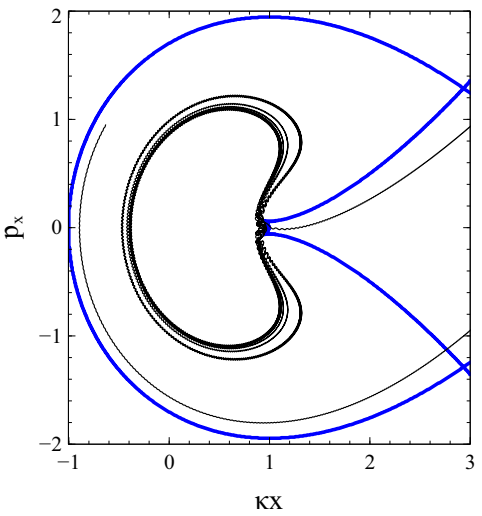

FIG. 3. Quasiregular trajectory (black curve) of the ion moving along a quasiclosed orbit within the region of regular trajectories and then escaping this region by crossing ℓ_5. Blue denotes the boundary of the region of allowed particle motion (outer curve) and ℓ_1-ℓ_5 curves.

Ions moving along regular trajectories fill closed curves in the Poincaré section; (ii) quickly scattered ions on transient trajectories fill some domain in the Poincaré section by random and sparse points (note the density of points is determined by the typical timescale between two successive crossings of $z = 0$ plane, and rapidly scattered ions can get quite small I_z corresponding to strongly elongated trajectories in the $(\kappa x, p_x)$ plane with long excursions between two $z = 0$ crossings); and (iii) ions moving along quasiregular trajectories cross $z = 0$

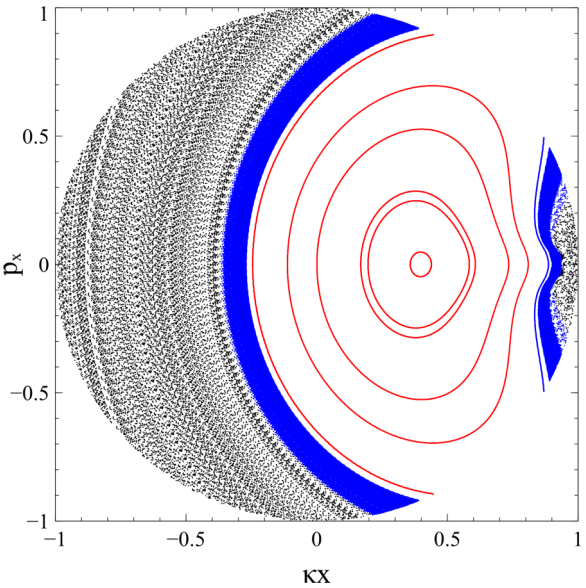

FIG. 4. Poincaré section of the system (2): The closed red curves denote particles moving along regular trajectories; black random sparse dots denote particles moving along transient trajectories; blue random dense dots denote particles moving along quasiregular trajectories, which cross ℓ_5.

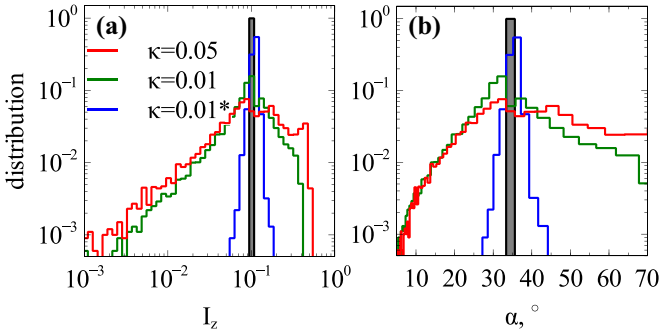

FIG. 5. Panel (a) shows I_z distributions and panel (b) shows pitch-angle distributions (we use pitch-angle values evaluated at the $z = 0$ plane): (red) $\kappa = 0.05$, (green) $\kappa = 0.01$, (blue) $\kappa = 0.01$, and Hamiltonian (2) contains $p_x^2/2$ instead of $(p_x - z + z^3/6)^2/2$. The initial distribution is shown by gray, whereas all colored distributions correspond to $\kappa t = 100$ simulation time.

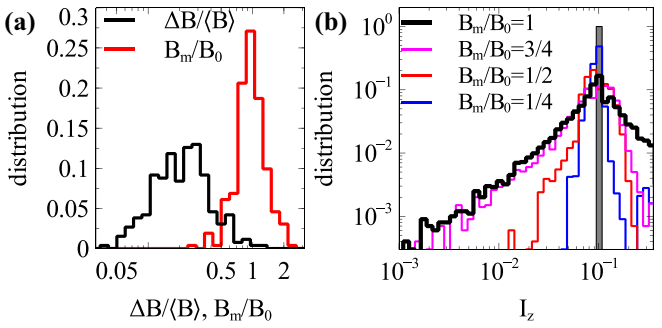

FIG. 6. (a) Distribution of characteristics of ion-scale discontinuities from Ref. [18] statistics: compressionality $\Delta B/\langle B\rangle$ (with $\Delta B = \max B - \min B$) and B_m/B_0. (b) I_z distributions for $\kappa = 0.01$ and different B_m/B_0. Gray denotes the initial I_z distribution.

with a short period (regular trajectories correspond to large I_z), but positions of crossings are randomly distributed. Figure 4 demonstrates that quasiregular trajectories (crossing ℓ_5) fill a layer separating regular trajectories and transient trajectories, but the total area of these quasiregular trajectories is smaller than the areas filled by both regular and transient trajectories.

IV. STATISTICS OF ADIABATIC INVARIANT JUMPS

Figure 2(b) shows that different sections of orbit crossing the separatrix are associated to quite different I_z values. This is an important property of the geometrical I_z destruction: Jumps $\langle\Delta I_z\rangle \sim 1$ do not depend on κ and are quite large, i.e., even for arbitrarily small κ the ion scattering is fast and effective. Note that $\kappa \to 0$ means the transition between rotational (with $B_n \neq 0$) and tangential ($B_n \to 0$) types of SWDs [44]. Figure 5 (left panel) shows evolution of initially narrow I_z distribution for two κ values: Geometrical jumps of I_z quickly widen I_z distributions. The scattering rate in the *slow time* κt does not depend on κ. However, the rotation period τ of particle motion in the $(\kappa x, p_x)$ plane is of order $1/\kappa$. This period determines the timescale of the ion interaction with the same SWD, i.e., after one separatrix crossing ions turn around at large κx and come back to the separatrix again after $\sim\tau$ period. Ion scattering and destruction of I_z is equivalent to the pitch-angle scattering, because I_z determines the ion pitch angle, e.g., at $z = 0$, $p_x = 0$ the ion pitch angle is defined as $\cos\alpha = \mathbf{v}\cdot\mathbf{B}/Bv = [\kappa x + \sqrt{2h - (\kappa x)^2}]/\sqrt{1+\kappa^2}$. Each trajectory in the $(\kappa x, p_x)$ plane is associated with some I_z value, and jump of I_z means change of trajectory. As each trajectory is characterized by some κx at $p_x = 0$ crossing, jumps of I_z result in changes of this κx [see Fig. 2(b)]. Thus, I_z jumps lead to values of κx at $p_x = 0$ jumps and to $\alpha = \alpha(\kappa x)$ jumps (note $h = \text{const}$ for ion scattering). Figure 5 (right panel) shows evolution of pitch-angle distributions recalculated from I_z distributions: Starting with a narrow α distribution, ions are quickly scattered and fill a broad α range.

To demonstrate the effect of magnetic field component B_m on ion scattering we compare I_z, α distributions obtained for Hamiltonian (2) with the $(p_x - z + z^3/6)^2$ term (B_m peak) and with the $p_x^2/2$ term ($B_m = 0$; classical compressional discontinuity, see Ref. [22]). Figure 5 shows that in the absence of B_m peak (i.e., when $B_m = 0$) the ion scattering is quite weak: I_z, α distributions are narrow peaks around the initial distribution (in agreement with theoretical predictions of slow I_z destruction, see Refs. [36,37]).

Although Fig. 1 shows almost force-free discontinuity ($B \approx \text{const}$), the B_m magnitude is slightly smaller than B_l magnitude, i.e., the field model $B_m^2 + B_l^2 = \text{const}$ in Hamiltonian (2) is an approximation. To study ion interaction with discontinuities having $B_m/B_0 < 1$ we consider statistics of ion-scale $L \sim d_i$ discontinuities from [18]. Figure 6(a) shows B_m/B_0 distribution and $\Delta B/\langle B\rangle$ (deviation from the force-free condition) for ~250 individual discontinuities: There is a significant fraction of $B_m/B_0 \in [0.5, 0.75]$ events, whereas for most of events $\Delta B/B \sim 0.03$. To examine how effect of strong I_z destruction depends on B_m/B_0 we plot I_z distributions for $\kappa t = 100$ simulation time and different B_m/B_0 values in Hamiltonian (2). For $B_m/B_0 > 0.75$ the I_z destruction rate is comparable to one for $B_m/B_0 = 1$, whereas for $B_m/B_0 < 0.75$ the I_z destruction rate is smaller and resulted I_z distribution is narrower. Therefore, the effect of the fast I_z destruction remains actual for a wide range of observed B_m/B_0 values. Note we consider rotational discontinuities that are typically Alfvenic-type structures with $B \approx \text{const}$ [10,18,31], but solar wind ions also interact with various compressional structures contributing to the solar wind magnetic field spectrum [45,46], e.g., mirror mode structures (e.g., Refs. [47,48]) and interplanetary shocks (e.g., Refs. [49–51]). Investigation of ion scattering by such structures (with $B_m/B_0 \ll 1$ and asymmetrical B_l profiles) deserves a separate study. An important element of compressional structures with the ion kinetic scales is a polarization electric field forming due to the decoupling of ion and electron motions (e.g., Ref. [52]). Such field almost absents in the force-free discontinuities [53] but can strongly influence ion scattering in compressional discontinuities [54]. Therefore, further investigations of ion interaction with partially force-free and compressional structures would require inclusion polarization fields into consideration.

V. DISCUSSION AND CONCLUSIONS

In Hamiltonian (2), κ determines the time interval between two scatterings [a timescale of one period of ion motion in the $(\kappa x, p_x)$ plane]. In systems with multiple SWDs, the timescale between scatterings would be partially controlled by the SWD occurrence rate, which does not depend on κ. This further reduces the importance of B_n (or κ) value for the ion scattering and makes separation between almost tangential (small but finite B_n) and rotational SWDs unimportant for determination of their role in ion scattering. Thus, we show that B_n amplitude (κ value) does not control the ion scattering rate in the presence of geometrical I_z destruction, i.e., ions are similarly scattered by rotational and almost tangential (with small, but finite B_n) SWDs.

This scattering is a universal mechanism for SWDs with the B_m peak comparable to the B_l magnitude (the most common configuration of compressionless SWDs, e.g., Refs. [1,10,19,42]) and sufficiently hot ions (or sufficiently thin SWDs; $L \sim \rho$). The condition $L \sim \rho$ can be rewritten for the ion energy $h/T_i \sim \beta_i (L/d_p)^2$ with T_i and β_i being solar wind temperature and the ratio of thermal and magnetic pressures. For most intense discontinuities $L/d_p \in [1, 10]$ [18–20] and typical $\beta_i \in [0.1, 10]$ (see Ref. [55]). Thus, almost all suprathermal solar wind population can be strongly scattered due to interaction with SWDs. This effect, together with scattering by plasma waves (e.g., Refs. [41,56]), should shape the observed low-anisotropic distribution of solar wind ions at 1 AU [55] and contribute to the quick cross-field transport of high-energy ion populations [12–14].

ACKNOWLEDGMENTS

We acknowledge the support NASA Contract No. NAS5-02099 for ARTEMIS data. The work of A.V.A., A.I.N., A.A.V., and A.A.V. was supported by the Russian Scientific Foundation, Project No. 19-12-00313. A.I.N. also acknowledges support from Leverhulme Thrust (Grant No. RPG-2018-143). The work of L.M.Z. was supported by the Russian Science Foundation (Grant No. 20-42-04418).

[1] B. T. Tsurutani and C. M. Ho, Rev. Geophys. **37**, 517 (1999).
[2] R. Bruno and V. Carbone, Liv. Rev. Solar Phys. **2**, 4 (2005).
[3] T. D. Phan, S. D. Bale, J. P. Eastwood, B. Lavraud, J. F. Drake, M. Oieroset, M. A. Shay, M. Pulupa, M. Stevens, R. J. MacDowall, A. W. Case, D. Larson, J. Kasper, P. Whittlesey, A. Szabo, K. E. Korreck, J. W. Bonnell, T. D. de Wit, K. Goetz, P. R. Harvey, T. S. Horbury, R. Livi, D. Malaspina, K. Paulson, N. E. Raouafi, and M. Velli, Astrophys. J. Sup. **246**, 34 (2020).
[4] T. Dudok de Wit, V. V. Krasnoselskikh, S. D. Bale, J. W. Bonnell, T. A. Bowen, C. H. K. Chen, C. Froment, K. Goetz, P. R. Harvey, V. K. Jagarlamudi, A. Larosa, R. J. MacDowall, D. M. Malaspina, W. H. Matthaeus, M. Pulupa, M. Velli, and P. L. Whittlesey, Astrophys. J. Sup. **246**, 39 (2020).
[5] J. A. Tessein, W. H. Matthaeus, M. Wan, K. T. Osman, D. Ruffolo, and J. Giacalone, Astrophys. J. Lett. **776**, L8 (2013).
[6] J. T. Gosling, Space Sci. Rev. **172**, 187 (2012).
[7] W. H. Matthaeus, G. Qin, J. W. Bieber, and G. P. Zank, Astrophys. J. Lett. **590**, L53 (2003).
[8] G. Zimbardo, P. Pommois, and P. Veltri, Astrophys. J. Lett. **639**, L91 (2006).
[9] J. R. Jokipii, Astrophys. J. **146**, 480 (1966).
[10] B. J. Vasquez, V. I. Abramenko, D. K. Haggerty, and C. W. Smith, J. Geophys. Res. (Space Phys.) **112**, A11102 (2007).
[11] J. E. Borovsky, Phys. Rev. Lett. **105**, 111102 (2010).
[12] J. Giacalone and J. R. Jokipii, Astrophys. J. **520**, 204 (1999).
[13] C. Pei, J. R. Jokipii, and J. Giacalone, Astrophys. J. **641**, 1222 (2006).
[14] J. Giacalone, J. R. Jokipii, and J. E. Mazur, Astrophys. J. Lett. **532**, L75 (2000).
[15] P. Sun, J. R. Jokipii, and J. Giacalone, Astrophys. J. **827**, 16 (2016).
[16] W. Horton, Physic. Rep. **192**, 1 (1990).
[17] V. Angelopoulos, Space Sci. Rev. **165**, 3 (2011).
[18] A. V. Artemyev, V. Angelopoulos, and I. Y. Vasko, J. Geophys. Res. (Space Phys.) **124**, 3858 (2019).
[19] J. J. Podesta, J. Geophys. Res. **122**, 2795 (2017).
[20] A. Greco, S. Perri, S. Servidio, E. Yordanova, and P. Veltri, Astrophys. J. Lett. **823**, L39 (2016).
[21] B. V. Chirikov, *Reviews of Plasma Physics*, 1st ed., Vol. 13 (Consultants Bureau, New York, 1987), pp. 1–92.
[22] J. Büchner and L. M. Zelenyi, J. Geophys. Res. **94**, 11821 (1989).
[23] H. U. Auster, K. H. Glassmeier, W. Magnes, O. Aydogar, W. Baumjohann, D. Constantinescu, D. Fischer, K. H. Fornacon, E. Georgescu, P. Harvey, O. Hillenmaier, R. Kroth, M. Ludlam, Y. Narita, R. Nakamura, K. Okrafka, F. Plaschke, I. Richter, H. Schwarzl, B. Stoll, A. Valavanoglou, and M. Wiedemann, Space Sci. Rev. **141**, 235 (2008).
[24] J. P. McFadden, C. W. Carlson, D. Larson, M. Ludlam, R. Abiad, B. Elliott, P. Turin, M. Marckwordt, and V. Angelopoulos, Space Sci. Rev. **141**, 277 (2008).
[25] B. U. Ö. Sonnerup and L. J. Cahill, Jr., J. Geophys. Res. **73**, 1757 (1968).
[26] V. Angelopoulos, P. Cruce, A. Drozdov, E. W. Grimes, N. Hatzigeorgiu, D. A. King, D. Larson, J. W. Lewis, J. M. McTiernan, D. A. Roberts, C. L. Russell, T. Hori, Y. Kasahara, A. Kumamoto, A. Matsuoka, Y. Miyashita, Y. Miyoshi, I. Shinohara, M. Teramoto, J. B. Faden, A. J. Halford, M. McCarthy, R. M. Millan, J. G. Sample, D. M. Smith, L. A. Woodger, A. Masson, A. A. Narock, K. Asamura, T. F. Chang, C.-Y. Chiang, Y. Kazama, K. Keika, S. Matsuda, T. Segawa, K. Seki, M. Shoji, S. W. Y. Tam, N. Umemura, B.-J. Wang, S.-Y. Wang, R. Redmon, J. V. Rodriguez, H. J. Singer, J. Vandegriff, S. Abe, M. Nose, A. Shinbori, Y.-M. Tanaka, S. UeNo, L. Andersson, P. Dunn, C. Fowler, J. S. Halekas, T. Hara, Y. Harada, C. O. Lee, R. Lillis, D. L. Mitchell, M. R. Argall, K. Bromund, J. L. Burch, I. J. Cohen, M. Galloy, B. Giles,

A. N. Jaynes, O. Le Contel, M. Oka, T. D. Phan, B. M. Walsh, J. Westlake, F. D. Wilder, S. D. Bale, R. Livi, M. Pulupa, P. Whittlesey, A. DeWolfe, B. Harter, E. Lucas, U. Auster, J. W. Bonnell, C. M. Cully, E. Donovan, R. E. Ergun, H. U. Frey, B. Jackel, A. Keiling, H. Korth, J. P. McFadden, Y. Nishimura, F. Plaschke, P. Robert, D. L. Turner, J. M. Weygand, R. M. Candey, R. C. Johnson, T. Kovalick, M. H. Liu, R. E. McGuire, A. Breneman, K. Kersten, and P. Schroeder, Space Sci. Rev. **215**, 9 (2019).

[27] T. Knetter, F. M. Neubauer, T. Horbury, and A. Balogh, J. Geophys. Res. **109**, A06102 (2004).

[28] A. Neishtadt, C. Simo, D. Treschev, and A. Vasiliev, Discr. Contin. Dyn. Syst. Ser. B **10**, 621 (2008).

[29] H. Karimabadi, P. L. Pritchett, and F. V. Coroniti, J. Geophys. Res. **95**, 17153 (1990).

[30] A. V. Artemyev, A. I. Neishtadt, and L. M. Zelenyi, Phys. Rev. E **89**, 060902(R) (2014).

[31] M. Neugebauer, J. Geophys. Res. **111**, A04103 (2006).

[32] L. D. Landau and E. M. Lifshitz, *Mechanics*, Course of Theoretical Physics Vol. 1 (Pergamon, Oxford, 1988).

[33] V. I. Arnold, V. V. Kozlov, and A. I. Neishtadt, *Mathematical Aspects of Classical and Celestial Mechanics*, 3rd ed., Dynamical Systems III. Encyclopedia of Mathematical Sciences (Springer-Verlag, New York, 2006).

[34] T. J. Birmingham, J. Geophys. Res. **89**, 2699 (1984).

[35] A. I. Neishtadt, Regul. Chaotic Dyn. **5**, 213 (2000).

[36] A. I. Neishtadt, Sov. J. Plasma Phys. **12**, 568 (1986).

[37] J. R. Cary, D. F. Escande, and J. L. Tennyson, Phys. Rev. A **34**, 4256 (1986).

[38] J. L. Tennyson, J. R. Cary, and D. F. Escande, Phys. Rev. Lett. **56**, 2117 (1986).

[39] L. M. Zelenyi, A. I. Neishtadt, A. V. Artemyev, D. L. Vainchtein, and H. V. Malova, Phys. Usp. **56**, 347 (2013).

[40] A. Neishtadt and D. Treschev, Ergodic Theory Dynam. Syst. **31**, 259 (2011).

[41] P. Hellinger, P. Trávníček, J. C. Kasper, and A. J. Lazarus, Geophys. Res. Lett. **33**, L09101 (2006).

[42] A. Tenerani and M. Velli, Astrophys. J. Lett. **867**, L26 (2018).

[43] D. L. Vainchtein, J. Büchner, A. I. Neishtadt, and L. M. Zelenyi, Nonlin. Process. Geophys. **12**, 101 (2005).

[44] P. D. Hudson, Plan. Sp. Sci. **18**, 1611 (1970).

[45] P. Veltri and A. Mangeney, in *American Institute of Physics Conference Series*, American Institute of Physics Conference Series Vol. 471, edited by S. R. Habbal, R. Esser, J. V. Hollweg, and P. A. Isenberg (American Institute of Physics, Melville, NY, 1999), pp. 543–546.

[46] P. Veltri, G. Nigro, F. Malara, V. Carbone, and A. Mangeney, Nonlin. Process. Geophys. **12**, 245 (2005).

[47] C. T. Russell, L. K. Jian, J. G. Luhmann, T. L. Zhang, F. M. Neubauer, R. M. Skoug, X. Blanco-Cano, N. Omidi, and M. M. Cowee, Geophys. Res. Lett. **35**, L15101 (2008).

[48] M. Volwerk, C. Goetz, F. Plaschke, T. Karlsson, and D. Heyner, Ann. Geophys. Discuss. **2019**, 1 (2019).

[49] L. B. Wilson III, A. Koval, A. Szabo, A. Breneman, C. A. Cattell, K. Goetz, P. J. Kellogg, K. Kersten, J. C. Kasper, B. A. Maruca, and M. Pulupa, Geophys. Res. Lett. **39**, L08109 (2012).

[50] E. L. M. Hanson, O. V. Agapitov, F. S. Mozer, V. Krasnoselskikh, S. D. Bale, L. Avanov, Y. Khotyaintsev, and B. Giles, Geophys. Res. Lett. **46**, 2381 (2019).

[51] I. J. Cohen, S. J. Schwartz, K. A. Goodrich, N. Ahmadi, R. E. Ergun, S. A. Fuselier, M. I. Desai, E. R. Christian, D. J. McComas, G. P. Zank, J. R. Shuster, S. K. Vines, B. H. Mauk, R. B. Decker, B. J. Anderson, J. H. Westlake, O. Le Contel, H. Breuillard, B. L. Giles, R. B. Torbert, and J. L. Burch, J. Geophys. Res. (Space Phys.) **124**, 3961 (2019).

[52] K. Schindler, J. Birn, and M. Hesse, Phys. Plasmas **19**, 082904 (2012).

[53] T. Neukirch, I. Y. Vasko, A. V. Artemyev, and O. Allanson, Astrophys. J. **891**, 86 (2020).

[54] E. Tsai, A. V. Artemyev, and V. Angelopoulos, Phys. Plasmas **24**, 012908 (2017).

[55] L. B. Wilson III, M. L. Stevens, J. C. Kasper, K. G. Klein, B. A. Maruca, S. D. Bale, T. A. Bowen, M. P. Pulupa, and C. S. Salem, Astrophys. J. Sup. **236**, 41 (2018).

[56] P. H. Yoon, J. Seough, C. S. Salem, and K. G. Klein, Phys. Rev. Lett. **123**, 145101 (2019).